Fusion Engineering and Design 191 (2023) 113535

Contents lists available at ScienceDirect

Fusion Engineering and Design

journal homepage: www.elsevier.com/locate/fusengdes

Electron Cyclotron stray radiation detector studies for JT-60SA

Alessandro Moro [a,*], Juan Ayllon [b], Lorenzo Figini [a], Saul Garavaglia [a], Ken Kajiwara [c], Takayuki Kobayashi [c], Carla Piccinni [d], Alessandro Simonetto [a], Carlo Sozzi [a], Hajime Urano [c], Maiko Yoshida [c]

[a] Institute for Plasma Science and Technology (ISTP-CNR), Italy
[b] University of Seville, Spain
[c] National Institutes for Quantum and Radiological Science and Technology, QST, Naka, Ibaraki 311-0193, Japan
[d] Max–Planck-Institut für Plasmaphysik, Boltzmannstrasse 2, D-85748 Garching bei München, Germany

ARTICLE INFO

Keywords:
Electron Cyclotron Resonance Heating
Stray radiation
Bolometer
Coating

ABSTRACT

Most of the present and future magnetic fusion devices rely on high power mm-waves injection for a variety of applications like plasma breakdown, heating and control. Since under specific operating conditions the mm-waves might not be fully absorbed, potentially damaging in-vessel components, the detection of the non-absorbed radiation is recommended. Among the options for stray radiation detection, we consider here the possibility to exploit the solid body bolometer and its use for JT-60SA. Analysis of the residual power fraction expected for low absorption plasma conditions is presented, considering the dependence on the Electron Cyclotron Resonance Heating (ECRH) system and plasma parameters of JT-60SA. The residual power hitting the wall is evaluated looking at direct illumination and cross-polarization effects. The possibility to integrate a sensor for EC stray radiation, adapting the solution of the detector developed for ITER, is the main outcome of this study. In the ITER bolometer the differential thermocouple principle is considered to single out the nuclear heating and the microwave loads. A key component of the detector is the metal body with a ceramic coating layer, optimized for 170 GHz and 60 GHz. Mm-waves characterization of different coating samples has been performed to identify the optimal solution for JT-60SA considering its multi-frequency ECRH system (138 GHz, 110 GHz, 82 GHz), and will be here presented. The experience from JT-60SA equipped with these sensors will be also useful for their future use in ITER.

1. Introduction

In the research plan of JT-60SA [1], the Electron Cyclotron Resonance Heating (ECRH) system will include up to 7 MW of installed power with the possibility to operate at three different frequencies, 138 GHz (100 s) 110 GHz (100 s) and 82 GHz (1 s). The use of the ECRH system, in particular in condition were low absorption might occur will result in EC stray radiation. The microwave power not absorbed by the plasma will not only diffuse in the form of diffuse radiation in the entire vacuum vessel but will also result in local thermal loads on in-vessel components. When EC radiation is injected as collimated beam in configurations prone to poor plasma absorption it can be either be refracted out or propagate unperturbed resulting in very high localized loads at the vessel components. After multiple reflections the final result is a diffuse stray radiation with much lower surface power density levels but affecting the overall vessel interior, reaching outer regions and vacuum windows via chamber openings. In this paper we report on the progress of a feasibility study for the design of a system to detect the amount of stray radiation. This study is presently based on the adaptation of the differential bolometers being developed for ITER to the JT-60SA device.

2. Stray radiation in JT-60SA

The initial research phase of JT-60SA will have installed two multi-frequency gyrotron units (1 MW each) and capable to provide EC power at 138 GHz, 110 GHz and 82 GHz in addition to two single-frequency gyrotron units (1 MW each) at 110 GHz [2]. Then, it will be enhanced to 9 multi-frequency gyrotron units (1 MW each), in total, in the integrated research phase. Analysis of the expected power density at specific vessel locations in Integrated Commissioning (IC) and first research phases, with beam data and CAD model represented the first step of the feasibility study, providing qualitative and quantitative evaluation of the expected residual power density in case of

* Corresponding author.
E-mail address: alessandro.moro@istp.cnr.it (A. Moro).

https://doi.org/10.1016/j.fusengdes.2023.113535
Received 24 October 2022; Received in revised form 5 January 2023; Accepted 1 February 2023
Available online 15 February 2023

ow absorption from the plasma. The radiation will be launched into the plasma using steerable antennas [3], for poloidal and toroidal injection. The launcher setup in the presently on going integrated commissioning is different, with simplified antennas to inject EC beams at fixed poloidal angle using HE_{11} waveguides with 60 mm diameter. This setup is shown in Fig. 1(left) where a poloidal section of JT-60SA vessel with ECH antenna is presented. In this configuration the peak radiation power density at distance z from the launched beam waist is given by $P(0,z) = 2P_0/(\pi\ w_x(z)\ w_y(z))$ [W/m^2] and describes the directional energy flux in terms of Poynting vector on the axis of the single beam for astigmatic beam. According to what is given in [4] and considering a generic distance from the Gaussian beam axis r_e as edge taper, the average radiation power density loading $P_{av} = P_0/(\pi\ r_e{}^2)$ can be related to the peak one for a give choice of r_e. For $r_e = 2\ w$ the relation simply reads as $P_{av} = 1/8\ P(0,z)$. The average radiation power density is estimated considering the whole transmitted power distributed over the projection of the beam on the chamber wall at the reflecting points and in case of EC injection with zero absorption the values of the expected power density at the first and second reflection at the vacuum vessel wall are summarized in Table 1. The projected area corresponding to w and $2\ w$ contour is also indicated corresponding to the inclusion of 0.8647 and 0.9997 fractional power of the incoming 1 MW beam considered. We can thus expect several MW/m^2 per injected beam, hitting the inner wall at the first reflection. The EC antenna setup considered for first plasma operations will consist of truncated waveguide (60.3 mm diameter), with no additional optics attached and thus providing a diverging, defocused beam (launched beam radius w_0 = 19.42 mm located at (R_A, z_A) = (5.21 m, 1.72 m), with w_0 defined as the distance from beam axis where the E-field amplitude drops to $1/e$ of the maximum value. In the same launching configuration the case of low density and low temperature JT-60SA plasma was considered, and beam tracing simulation with the GRAY code [5] have been performed. As representative of possible plasma equilibrium and compatible with pre-ionization and EC-assisted breakdown phases, the circular cross section of Fig. 1 (right) was used. With plasma density in the range [10^{17} m^{-3}, 10^{19} m^{-3}] and electron temperature in the range [0.1 keV, 1 keV], the power densities listed in Table 2 were obtained. In this configuration the worst situation is found obviously at the first bounce, with values not too much different from those corresponding to the previous configuration without plasma, except for the cases with n = 10^{19} m^{-3} and T = 1 keV. As the plasma density increases, the diffraction effects would also result in the form of a different reflection point at the vacuum vessel locations, enlarging the region of direct illumination.

Analysis of the non-absorbed EC power fraction after 1 and 2 passes across the plasma has been done also for the First Research phase and the simulation done for plasma Scenario 4 (central temperature $T_{e,0}$ = 8 keV) is shown in Fig. 2). Ordinary Mode at the second harmonic is launched perpendicularly injected and the full poloidal scan achievable with the steering launcher [6] is considered. The color and the size of the symbols represent the residual P/P_0 value. The most exposed vessel area in this case is the top of the vessel due to the residual after the first pass (with areas illuminate by half of the initially injected EC power), which on the one hand is an unlikely direction of launch, on the other hand the area can be reached with significant amount of power in case the fraction of cross-polarization is considered, deflected at the density cut-off [7].

3. The differential thermocouple detector

The use of bolometers to detect radiation in tokamak environment is well established but in order to detect EC stray radiation a single bolometer in an environment with concurring heating parameters like plasma radiation, neutron and gamma heating can be not effective due to the large uncertainty of the measure. In the case of ITER, the goal is to measure EC stray radiation inside the vessel to optimize the ECH

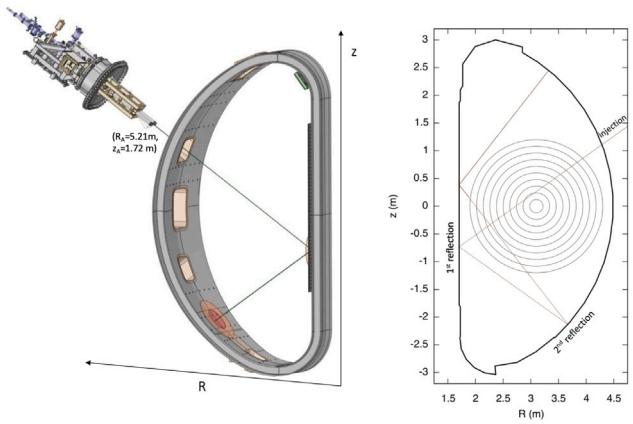

Fig. 1. Left: Layout of the optical system. Right: Beam trajectory considered for the analysis of stray load on vacuum vessel locations corresponding to 1st and 2nd reflection. The black circles represent the magnetic flux surfaces of the hypothetic circular plasma cross section considered for EC-assisted breakdown simulation with plasma axis at R_{ax} = 3.1 m, z_{ax} = 0 m and minor radius a = 1.2 m.

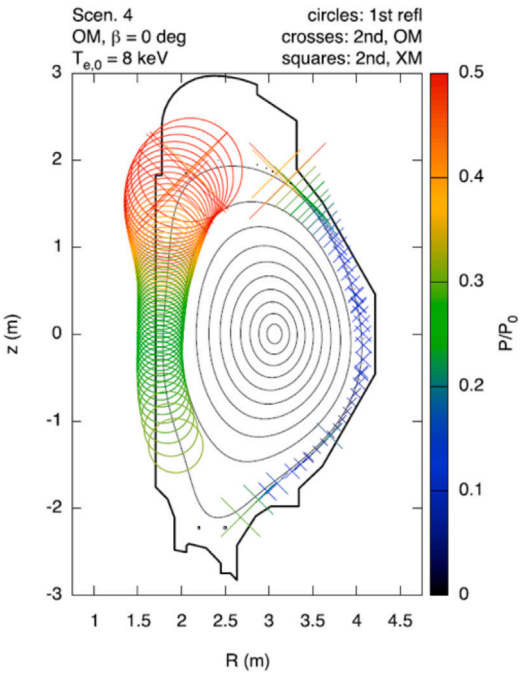

Fig. 2. Angular distribution of the non-absorbed EC radiation after one and two passes across the plasma considering the range of the poloidal injection angles given by the steering antenna. The symbols size is a visual hint for the amount of non-absorbed power: larger symbols indicate beam exit points with larger residual power. After first reflection, both polarizations contributions are represented for the following ones, with crosses for OM and squares (minimal contribution) for XM.

Table 1
Direct irradiation effects in terms of peak and average radiation power density (MW/m^2, 1 MW beam, simplified geometry, no plasma absorption, incidence angle α).

f [GHz]	1st bounce α = 35.5°		2nd bounce α = 8.9°	
	$P(0, z)$	P_{ave}	$P(0, z)$	P_{ave}
82	7.7	0.96	3.85	0.48
110	13.8	1.73	16.92	0.87
138	21.59	2.7	10.86	1.36

Table 2
Peak and average power density (MW/m^2, 1 MW beam) at the first reflection considering different plasma density, temperature and optical depth τ. The relation between τ and absorbed power is given by $P_{abs} = P_0\ (1-e^{-\tau})$, with $\tau \gtrsim 2.3$ required to have $\gtrsim 0.9$ absorption.

f [GHz]	n [10^{19} m^{-3}]	T [keV]	τ	$P(0, z)$	P_{ave}
82	0.01	0.1	1.7 10^{-3}	7.69	0.96
	0.1	0.3	5.4 10^{-2}	7.32	0.91
	1.0	1.0	1.17	2.37	0.3
110	0.01	0.1	5.2 10^{-3}	13.74	1.72
	0.1	0.3	1.6 10^{-1}	11.72	1.46
	1.0	1.0	5.34	0.07	0.01
138	0.01	0.1	5.0 10^{-3}	21.49	2.69
	0.1	0.3	1.6 10^{-1}	8.49	2.31
	1.0	1.0	4.96	0.14	0.02

operations and to minimize the heat loads on in-vessel components. The system is a passive component (not intended for machine protection), with advantages with respect to sniffer probes, requiring waveguide and vacuum extension to have the detector in radiation safe condition for example, and pyrodetectors, not compatible with neutron and gamma radiation. An alternative solution to overcome this issue is the differential thermocouple configuration. This setup (shown in 3 with a schematic representation) originates from Eindhoven University [8,9] and has been further developed as EC sensor for ITER. It relies on the microwave heating affects differently two bolometers, one of which has a ceramic coating on top. A second bolometer has no coating and reflects most of the incoming microwave power. As a result, the temperature difference between the bodies will be due to microwave heating, as the equal volumetric neutron heating is shared. This temperature difference will be measured with a differential thermocouple to single out the nuclear heating and the microwave loads. The Seebeck effect[1] is responsible of the direct conversion of temperature gradient to electric voltage. Despite the features and the design of the ITER sensor is out of the scope of this paper, which is focused on its possible integration into JT-60SA, the functionality of the detector is described with a thermal model, used to calculate the thermal contact conductances of the connections between different parts of the bolometers. These are identified with a number of nodes and heat transfer coefficients (in W/m^2/K) are defined according to the nature of the contact between those parts. An algorithm has been then developed to correlate the measured ΔV to ΔT and thus to the ECH power. According to the time scale considered (transient phases or stationary phase where radiation and conduction play an important role) the accuracy of the measurement can cover a wide range of power densities, from few tens of kW/m^2 up to 100 kW/m^2 with response time of the order of 0.3 s–1 s using $\Delta T/\Delta t$, T_{abs} at relatively low temperature and short time scales, increasing to 10 s–15 s if thermal equilibrium is considered.

4. Design integration

In the case of JT-60SA and its initial research phase, with available EC power and plasma scenarios a sensor for the stray radiation should be capable to detect power density as low as 7.5 kW/m^2 up to 2 MW/m^2 in steady state and transients up to 4 MW/m^2 for 5 s, with 3 kW/m^2 total radiation from plasma at the back of first wall [10]. Considering the achievable small dimensions that a sensor for the stray radiation might have (in the case of the ITER sensor a volume V = 61.4 × 31 × 16 mm^3) we could identify a possible location for a similar sensor inside JT-60SA that would take advantage of the presence of the stabilizing plate tiles to avoid the exposure to the plasma of the whole detector while ensuring the collection of the stray radiation with the active part of the sensor, given by the two upper surfaces of the cylinder bolometers. A diameter of few mm can fit the gaps between the tiles of the stabilizing plate, and location in the vessel can be selected. A preferred option is thus the one with sensors located close to ECH ports sectors (that for the Integrated commissioning and First Research phase will be Port 8 and Port 11), in the low field side of the vessel (to ease and minimizing the cabling) and in proximity of thermocouples, so that the additional information on the heating rate $\Delta T/\Delta t$ and absolute temperature T_{abs} might be available. This option is strongly intertwined to the stabilizing plate, actually under procurement for the first enhancement phase of JT-60SA, as shown in Fig. 4, where red circles are used to enlight the possible sensor location. A second option with lower impact on enhancement schedule and requiring a different integration in the vacuum vessel is also considered. In this alternative option the sensor is proposed to be installed within ports with available volume. In particular, ports P1 and P4 that will host EC launchers offer the chance of sensor installation and proof of principle of the detector, since no direct illumination by EC beams will be achieved, but only a measure of the diffuse stray radiation. Following the methodology found in [11] this amount is expected to be approximately few kW/m^2. Also in this alternative option, having a sensor in proximity of thermocouples would be beneficial.

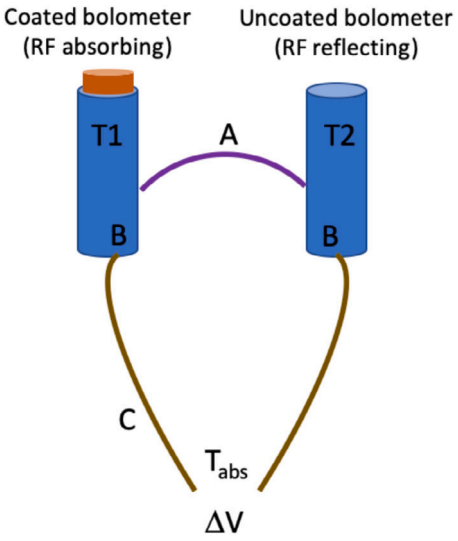

Fig. 3. Differential thermocouple arrangement.

5. Coating characterization

The ceramic coating is the most critical parameter for the performance of the sensor, since the material properties and the dielectric losses due to the interaction with electromagnetic waves will be used to determine the amount of stray radiation in proximity of the sensor itself. As a guideline driven by the development of the ITER sensor, the same power fraction absorption $A_{abs} = 0.8$ is initially chosen as a target for the candidate material. The risk to have larger values of $\Delta T/\Delta t$ in such absorbing coating in case of collimated beam is reduced as as far as the present proposal for JT-60SA is concerned, the bolometers are proposed to be located in low field side areas, either in sectors where EC is injected or in more distant once and where second reflection will occur. The assessment of the heating rate for different power densities will be part of the future work on sensor characterization Absorption in the ceramic is essentially a single-pass surface phenomenon in high-loss materials, becoming resonant and thickness-dependent in low-loss ones. Adapting to the present case the most general model for homogeneous,

[1] For the configuration of Fig. 3, the bolometers temperatures T_1 and T_2 result in electric voltage determined by the Seebeck coefficients of the connectors materials S_A and S_C, typically Ni-Si alloy and copper, according to $\Delta V = (S_A - S_C)\ (T_1 - T_2)$.

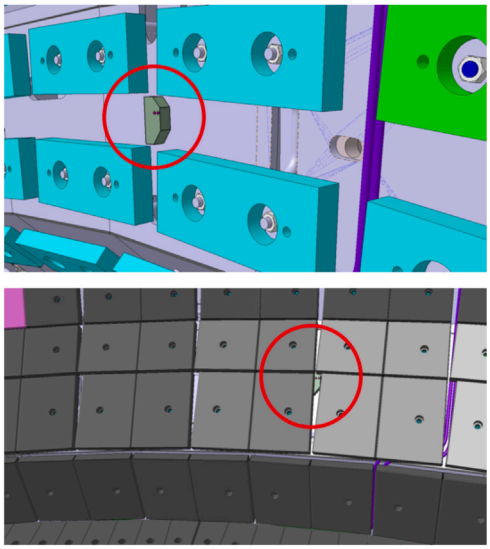

Fig. 4. A sketch of the sensor for EC stray integrated into the stabilizing plate of JT-60SA (top) and in the shadow on the stabilizing plate carbon tiles (bottom). The presence of tile gaps ensure the required field of view for the active parts of the detectors.

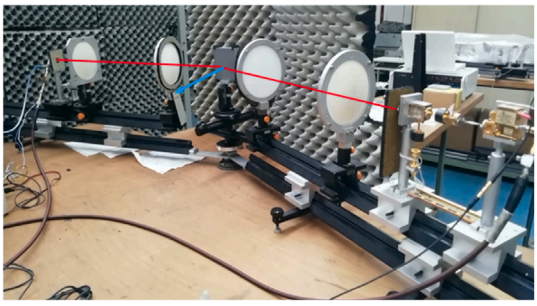

Fig. 5. Optical system and VNA instrumentation setup for low power measurements at ISTP-CNR Milano, as in [12]. The red lines (beam axes, with source at the right and receiver at the left) and the blue line (normal vector to the coating sample surface) represent the incidence plane.

linear, isotropic, conductive materials [12], propagation in the ceramic is described with inhomogeneous plane waves using the complex Snell law. In dedicated campaign measurements in the lab [13] and in the test facility MISTRAL [14,15] the required attenuation factor could indeed be achieved over a broad frequency range (see [16] and references therein), providing a basis to develop mm-wave stray radiation absorbers and allowing the design of the bolometer diagnostic to detect levels of stray radiation. In JT-60SA case the search is thus made with dedicated measurements of different coating samples (the same as [13], courtesy of ITER Organization and Stuttgart University), considering three ceramic materials with given thicknesses. A set of 19 samples with different ceramic coating thickness (including Al_2O_3-TiO_2, Cr_2O_3 and TiO_2 with thicknesses ranging from 30 μm to 250 μm) have been characterized using the setup of [12] made of confocal telescopes and a Vector Network Analyzer for low power measurements at ISTP-CNR Milano, as shown in Fig. 5. This to provide adapted coated cylinder specifications (material and thickness) for integration into the ITER prototype detector. Monostatic measurements were made at normal incidence and bistatic ones at different angles of incidence (ranging from 25° to 65°). Both TE and TM polarizations have been considered in the bistatic case. Both W and G-band were measured to cover the 63–112 and 136–220 GHz frequency ranges.

Only very preliminary data analysis has been performed so far on a selection of Al_2O_3-TiO_2 samples compound material, with a ratio of the Aluminium-Titanium compound equals to 60%/40% (additional information on can be found in [13] where the analysis carried out at 170 GHz for the same samples has been documented). The measured permittivity is approximately $\epsilon = \epsilon' - j\epsilon'' = 29 - j18$ in the W-band [75 to 110 GHz] and $30.0 - j\ 16.0$ in the G-band [140 to 220 GHz] respectively, obtained best fitting the collected data in the parameters space that includes ϵ', ϵ'' and thicknesses. Once the material permittivity is inferred, the reflectivity as a function of thickness and for a given frequency can be evaluated. Adapting to the present case the most general model for homogeneous, linear, isotropic, conductive materials [17] a value of 0.8 for $A_{abs} = 0.8$ could be obtained in the case of Al_2O_3-TiO_2 and normal incidence with approx 0.1 mm thickness at 138 GHz. Assuming that the dielectric constant of the material does not vary appreciably, the resonant thickness providing maximum absorption at 82 GHz would be larger by the ratio of the correspondent wavelengths. More details and results of the analysis of the complete set of ceramic coatings will be given a separate publication when the analysis is completed.

The development of this electro-magnetic absorbing coating for JT-60SA will end up with the definition of the best coating composition, the substrate preparation and the deposition process and measure its absorption performances. Additional tests have been identified to characterize the adapted sensor. As mentioned in 3 measuring the heating rate as a function of T_{abs} for example can be used to get the one-to-one relation between incident P_{den} and $\Delta T/\Delta t$, existing at any bolometer temperature, since $\Delta T/\Delta t = P_{abs}/(m\ c_v)$. A heat gun load can be considered thermally the same as applying a microwave load, resulting in a voltage between the output terminals.

6. Conclusions

The status of a feasibility study for EC stray radiation detector for JT-60SA is presented. The study covers analysis of the residual EC radiation in different configurations, adaptation of differential thermocouples bolometer developed for ITER, including the coating characterization for the absorbing properties of the detector. The Author would like to thank the colleagues at ITER Organization and Stuttgart University for the information provided on the ITER sensor design and for the coating samples provision that allowed us to perform the low power measurements at ISTP-CNR Milan laboratory.

Declaration of competing interest

The authors declare that they have no known competing financial interests or personal relationships that could have appeared to influence the work reported in this paper.

Data availability

Data will be made available on request.

Acknowledgments

This work has been carried out within the framework of the EUROfusion Consortium, funded by the European Union via the Euratom Research and Training Programme (Grant Agreement No 101052200 - EUROfusion). Views and opinions expressed are however those of the author(s) only and do not necessarily reflect those of the European Union or the European Commission. Neither the European Union nor the European Commission can be held responsible for them.

References

[1] Y. Kamada, et al., http://dx.doi.org/10.1088/1741-4326/ac10e7.
[2] T. Kobayashi, et al., Nucl. Fusion 62 (2022) 026039, http://dx.doi.org/10.1088/1741-4326/ac42f4.
[3] T. Kobayashi, et al., Fusion Eng. Des. 84 (2009) 1063–1067.
[4] P.F. Goldsmith, Quasi-optical techniques, Proc. IEEE 80 (11) (1992) 1729–1747.
[5] D. Farina, A quasi-optical beam-tracing code for electron cyclotron absorption and current drive: GRAY, Fusion Sci. Technol. 52 (2007) 154.
[6] P. Platania, et al., AIP Conf. Proc. 1689 (2015) 090010, http://dx.doi.org/10.1063/1.4936547.
[7] C. Sozzi, et al., http://ocs.ciemat.es/EPS2019PAP/pdf/P4.1089.pdf.
[8] N. Maassen, Microwave detector design for ITER, internship science and technology of nuclear fusion, eindhoven university of technology, Appl. Phys. 14 (2014) https://research.tue.nl/en/publications/eeb0de62-451f-4d11-bed0-2edc4440a9df.
[9] K. Arts, Electromagnetic and thermal design of the ITER microwave bolometer detector, internship science and technology of nuclear fusion, eindhoven university of technology, Appl. Phys. (2015) https://research.tue.nl/en/publications/0b497b8e-e283-4a9b-b22b-bcae552d0f64.
[10] M. Wanner, Plant Integration Document, https://users.jt60sa.org/?uid=222UJY.
[11] A. Moro, et al., Electron cyclotron stray radiation detection and machine protection system proposal for JT-60sa, Fusion Eng. Des. 123 (2017) http://dx.doi.org/10.1016/j.fusengdes.2017.03.028.
[12] A. Simonetto, et al., JINST 16 (2021) P03036, http://dx.doi.org/10.1088/1748-0221/16/03/P03036.
[13] A. Hentrich, et al., Resonant atmospheric plasma-sprayed ceramic layers effectively absorb microwaves at 170 GHz, J. Infrared Millim. Terahertz Waves 43 (2022) 349–365, http://dx.doi.org/10.1007/s10762-022-00861-7.
[14] S. Ullrich, et al., 140 GHz test chamber for stray electron cyclotron radiation, Stellarator News 98 (2005).
[15] M. Hirsch, H.P. Laqua, D. Hathiramani, et al., The impact of microwave stray radiation to in-vessel diagnostic components, AIP Conf. Proc. 1612 (2014) 39, http://dx.doi.org/10.1063/1.4894022.
[16] H. Meister, et al., JINST 14 (2019) C10004, http://dx.doi.org/10.1088/1748-0221/14/10/C10004.
[17] C.A. Balanis, Advanced Engineering Electromagnetics, John Wiley & Sons, 1989.